Eng.& Tech. Journal,Vol.30, N0.6, 2012

Deflection Estimation of Un-Symmetric Isotropic Cam with Three Circular-Arc Contact Profiles

Dr. Louay Sabah Yousuf
Engineering College, Baghdad University
Email: louaysabah79@yahoo.com

Received on: 9/8/2011 & Accepted on: 1/3/2012

ABSTRACT

In this paper the principal objectives is to design a suitable profile that produces minimum value of jerk and contact stress keeping the acceleration within a limit especially in high-speed machine. Many works in the experimental part are done on the synthesis of cam profile in accuracy and system flexibility on the output follower motion; but there is a lack in the analytical part. The analytical formulation has been done with classical plate theory of un-symmetric cam with three circular-arc contact profiles using the equation of circular plate solution due to the distributed load comes from the perpendicular contact harmonic motion of the follower. The cam used in the paper can be found in cutting and metal forming tools, heavy duty of marine engine, and fast manufacturing equipment. The aim of the present paper is to calculate the maximum deflection on cam boundaries varying with (r and θ) coordinates between beginning and ending of contact follower loadings. The results were classified into mathematical model and finite element using software ANSYS.

Keywords: Cam Profile, Contact Loading, Circular Plate, Finite element, Un-symmetric Cam.

تخمين التشوه للحدبة الايزوتروبيكية غير المتناظرة بوجود ثلاث اقواس تماس – دائرية لهيئته

الخلاصة:

ان المبدء الرئيسي في هذا البحث هو التصميم المناسب للهيئة والذي ينتج عنه اقل قيمة للجيرك والاجهاد الملامس بحيث يحافظ على التعجيل ضمن الحدود الخاصة في السرع العالية للماكنة. نفذت العديد من البحوث في الجانب العملي على تركيب الشكل الخارجي لهيئة الحدبة في دقة ومرونة نظام الحركة الخارجية للتابع، ولكن يوجد هناك نقص في الجانب النظري. ان الصيغة النظرية نفذت بنظرية الصفيحة الكلاسيكية للحدبة غير المتناظرة بثلاث اقواس دائرية للهيئة الملامسة باستخدام حل معادلات الصفيحة الدائرية نتيجة للحمل الموزع القادم من تعامد الحركة الهارمونيكية الملامسة للتابع. ان الحدبة المستخدمة في هذا البحث يمكن تواجدها في مكائن القطع والتشكيل، مكائن العمل الثقيلة، ومعدات التصنيع السريعة. ان الهدف من هذا البحث هو حساب اكبر تشوه على حدود الحدبة متغيرة مع الاحداثيات (r and θ) بين بداية ونهاية الحمل الملامس للتابع. النتائج تم تصنيفها الى موديل رياضي وطريقة العناصر المحددة باستخدام برنامج طريقة العناصر المحددة (ANSYS).

https://doi.org/10.30684/etj.30.6.7
2412-0758/University of Technology-Iraq, Baghdad, Iraq
This is an open access article under the CC BY 4.0 license http://creativecommons.org/licenses/by/4.0

Nomenclatures:

Normal Letters		
Symbol	**Definition**	**Unit**
a	Major distance of Hertzian contact axis	m
b	Minor distance of Hertzian contact axis	m
a_1	Major distance of ellipse axis	m
b_1	Minor distance of ellipse axis	m
a_2	Difference radius of curvatures between ellipse and semi-circle centers	m
C	Particular solution constant	-----------
D	Bending rigidity	N. m
E_1, E_2	Modulus of elasticity for both cam and follower	$\frac{N}{m^2}$
L	Length of simply-supported beam	m
L_1	Difference length between two points of contact	m
m, n	Functions of the geometry of the contact surfaces	-----------
m_1	Single trigonometric of Furrier series	------------
M_r, M_θ, and $M_{r\theta}$	Circular plate bending and twist moment	N.m
	Maximum contact pressure	
P	Total contact load	
r, and θ	Polar coordinates	m, Rad
	Radius of clamped cam center	m
R_1, R_1'	Wheel radius of Curvature	m
	Head radius of Curvature	m
q	Loading contact per unit length	$\frac{N}{m}$
W	Circular plate deflection	m
x, y	Cartesian coordinates	m
Greek Letters		
Symbol	**Definition**	**Unit**
	Yield Stress	$\frac{N}{m^2}$
	Constant (3.1416)	---------
	Angle between the planes containing curvatures	Degree
ν_1, ν_2	Poisson's ratio for both cam and follower	---------
α	Angle depend upon the functions geometry m, n	Degree
θ_1, θ_2	Angles of the beginning and the ending for both flanks and noses	Rad, Rad

INTRODUCTION

A shape optimization of a two-dimensional cam profile that produces minimum values of jerk and contact stress is designed in a heavily constrained environment keeping the peak values of acceleration within a

PDF created with pdfFactory Pro trial version www.pdffactory.com

limit based on genetic algorithm and fuzzy membership function by using classical splines of 6-, 7-, and 8-orders and B-splines of 6-and 8-orders for the polynomial mod traps spline curves of control point parameters, [1,2, 3]. Moreover the fatigue life and microscopic edge cracks for two open-celled foamed polymers having different densities is measured in compression impact using a cam-driven compound pendulum system and observed that the material measurements at constant incident energy included the static compression modulus and peak dynamic stress, which progressively degraded as the number of impacts approached one million, [4]. On the other hand the optimum displacement curve is found for which cam-follower velocity curve, acceleration curve, dynamic response of jerk, pressure angle, induced force and stress of experimental outputs to be continuous and their peak values as small as possible on both the rising and the falling motion of the cam-follower with changing the control points of degree three and six which used in B-spline polynomial by using advanced techniques for data acquisition and data processing, [5, 6, 7]. A synthesis method is described for designing flexible cam profile of marine engine with just one revolving scan of the profile and analyzed the minimum zone criterion of the form deviation error of disc cam by using smoothing cubic spline curves interpolation for specifying maximum and minimum distance between two curves, [8, 9]. The aim of the present paper is to calculate the maximum deflection on cam boundaries varying with (r, and θ) coordinates between beginning and ending of contact follower loadings.

ANALYTICAL PROCEDURE:

Higher values of acceleration and jerk of the cam-follower driven system are never desirable as these affect smoothness of operation of the system and generate force that induces high contact stress on the cam surface. In this study of general contact loading case, assuming elastic and isotropic material behavior, Hertz showed that the intensity of pressure between the contacting surfaces could be represented by the elliptical (or, rather, semi-ellipsoid) construction shown in Fig. 1, [10]. Maximum contact pressure (P_o) for shakedown of the contact region is:

$$P_o = 0.6 * \sigma_y \qquad .....(1)$$

And the total contact load is given by the volume of the semi-ellipsoid, [10]:

i.e. $$P = \frac{2*\pi*a*b*P_o}{3} \qquad ....(2)$$

Where:

$$a = m * [\frac{3*P*\Delta}{4*A_1}]^{1/3}, \quad b = n * [\frac{3*P*\Delta}{4*A_1}]^{1/3}$$

And;

$$A_1 = \frac{1}{2} * [\frac{1}{R_1} + \frac{1}{R_1'} + \frac{1}{R_2} + \frac{1}{R_2'}] \qquad .....(3)$$

$$\Delta = \frac{1}{E_1} * (1 - \nu_1^2) + \frac{1}{E_2} * (1 - \nu_2^2) \qquad ....(4)$$

For flat-sided R_1 will be the wheel radius and R_1' will be infinite. Similarly for railway lines with head radius R_2 the value of R_2' will be infinite to produce the flat length of radii.

Also;

$\psi = 90^o$, because the contact load is perpendicular to the cam profile.

i.e;

PDF created with pdfFactory Pro trial version www.pdffactory.com

$\alpha = \cos^{-1}(\frac{B_1}{A_1})$

Also;

$$B_1 = \frac{1}{2} * [\left(\frac{1}{R_1} - \frac{1}{R_1'}\right)^2 + \left(\frac{1}{R_2} - \frac{1}{R_2'}\right)^2 + 2 * \left(\frac{1}{R_1} - \frac{1}{R_1'}\right) * \left(\frac{1}{R_2} - \frac{1}{R_2'}\right) * \cos(2 * \psi)]^{\frac{1}{2}} \quad (5)$$

According to the value of angle (α), it can be found the value of n, m from Table (1), [11]:

Table (1) The value of angle (α) against the values of m, and n.

α (degree)	**20**	**30**	**35**	**40**	**45**	**50**	**55**	**60**
m	**3.778**	**2.731**	**2.397**	**2.136**	**1.926**	**1.754**	**1.611**	**1.486**
n	**0.408**	**0.493**	**0.530**	**0.567**	**0.604**	**0.641**	**0.678**	**0.717**

α (degree)	**65**	**70**	**75**	**80**	**85**	**90**
m	**1.378**	**1.284**	**1.202**	**1.128**	**1.061**	**1**
n	**0.759**	**0.802**	**0.846**	**0.893**	**0.944**	**1**

From the circular plate equation as a function of (r, and θ) coordinates is,[12]:

$$\left(\frac{\partial^2}{\partial r^2} + \frac{2}{r}\frac{\partial}{\partial r}\right) * M_r + \left(-\frac{1}{r}\frac{\partial}{\partial r} + \frac{1}{r^2}\frac{\partial^2}{\partial \theta^2}\right) * M_\theta$$

$$+ \left(-\frac{2}{r}\frac{\partial^2}{\partial r\,\partial \theta} - \frac{2}{r^2}\frac{\partial}{\partial \theta}\right) * M_{r\theta} + q = 0, [12] \quad .....(6)$$

Where:

For isotropic plate, the bending and twist moments are, [12]:

$$M_r = -D * [\frac{\partial^2 w}{\partial r^2} + \nu * (\frac{1}{r}\frac{\partial w}{\partial r} + \frac{1}{r^2}\frac{\partial^2 w}{\partial \theta^2})]$$

$$M_\theta = -D * [\left(\frac{1}{r}\frac{\partial w}{\partial r} + \frac{1}{r^2}\frac{\partial^2 w}{\partial \theta^2}\right) + \nu * \frac{\partial^2 w}{\partial r^2}]$$

$$M_{r\theta} = D * (1 - \nu) * [\frac{1}{r}\frac{\partial^2 w}{\partial r\,\partial \theta} - \frac{1}{r^2}\frac{\partial w}{\partial \theta}]$$

The value of first term of eq. (6) is:

PDF created with pdfFactory Pro trial version www.pdffactory.com

$$\left(\frac{\partial^2}{\partial r^2}+\frac{2}{r}\frac{\partial}{\partial r}\right)*M_r = -D*\left(\frac{\partial^4 w}{\partial r^4}+\frac{\nu}{r}\frac{\partial^3 w}{\partial r^3}+\frac{\nu}{r^2}\frac{\partial^4 w}{\partial r^2\,\partial\theta^2}-\frac{2*\nu}{r^3}\frac{\partial^3 w}{\partial r\,\partial\theta^2}+\frac{2}{r}\frac{\partial^3 w}{\partial r^3}+\frac{2*\nu}{r^4}\frac{\partial^2 w}{\partial\theta^2}\right)$$

And the value of second term of eq. (6) is:

$$\left(-\frac{1}{r}\frac{\partial}{\partial r}+\frac{1}{r^2}\frac{\partial^2}{\partial\theta^2}\right)*M_\theta = -D*\left(-\frac{1}{r^2}\frac{\partial^2 w}{\partial r^2}+\frac{1}{r^3}\frac{\partial w}{\partial r}+\frac{2}{r^4}\frac{\partial^2 w}{\partial\theta^2}-\frac{\nu}{r}\frac{\partial^3 w}{\partial r^3}+\frac{1}{r^4}\frac{\partial^4 w}{\partial\theta^4}+\frac{\nu}{r^2}\frac{\partial^4 w}{\partial r^2\,\partial\theta^2}\right)$$

Also the value of third term of eq. (6) is:

$$\left(-\frac{2}{r}\frac{\partial^2}{\partial r\,\partial\theta}-\frac{2}{r^2}\frac{\partial}{\partial\theta}\right)*M_{r\theta} = D*\left(-\frac{2}{r^2}\frac{\partial^4 w}{\partial r^2\,\partial\theta^2}+\frac{2}{r^3}\frac{\partial^3 w}{\partial r\,\partial\theta^2}-\frac{2}{r^4}\frac{\partial^2 w}{\partial\theta^2}+\frac{2*\nu}{r^2}\frac{\partial^4 w}{\partial r^2\,\partial\theta^2}-\frac{2*\nu}{r^3}\frac{\partial^3 w}{\partial r\,\partial\theta^2}+\frac{2*\nu}{r^r}\frac{\partial^2 w}{\partial\theta^2}\right)$$

It can be put the three terms derived above in eq. (6) to obtain:

$$\frac{\partial^4 w}{\partial r^4}+\frac{2}{r}\frac{\partial^3 w}{\partial r^3}-\frac{1}{r^2}\frac{\partial^2 w}{\partial r^2}+\frac{1}{r^3}\frac{\partial w}{\partial r}+\frac{2}{r^2}\frac{\partial^4 w}{\partial r^2\,\partial\theta^2}-\frac{2}{r^3}\frac{\partial^3 w}{\partial r\,\partial\theta^2}+\frac{4}{r^4}\frac{\partial^2 w}{\partial\theta^2}+\frac{1}{r^4}\frac{\partial^4 w}{\partial\theta^4}=\frac{q}{D} \quad \ldots\ldots(7)$$

The homogenous solution of eq. (7) is, [13]:

$$w(r,\theta)_H = \sum_{m_1=1,3,5}^{\infty}[R_m*\sin(m*\theta)+R'_m*\cos(m*\theta)]$$

Put the homogenous solution in eq. (7) to obtain:

$$w(r,\theta)_H = \sum_{m=1,3,5}^{\infty}[(A_m*r^m+B_m*r^{-m}+C_m*r^{m+2}+D_m*r^{m-2})*\sin(m*\theta)+(A'_m*r^m+B'_m*r^{-m}+C'_m*r^{m+2}+D'_m*r^{m-2})*\cos(m*\theta)]$$

For un-symmetric cam the deflection, slope, and the moment must be infinite at the center of the plate, then the homogenous will become:

$$w(r,\theta)_H = \sum_{m=1,3,5}^{\infty}[(A_m*r^m+C_m*r^{m+2})*\sin(m*\theta)+(A'_m*r^m+C'_m*r^{m+2})*\cos(m*\theta)]$$

Apply the infinite series on the homogenous solution as below:

$$(r^m*\sin(m*\theta)) = (1+r+r^2+r^3+r^4+r^5+\cdots)*\left(m*\theta-\frac{(m*\theta)^3}{3!}+\frac{(m*\theta)^5}{5!}-\cdots\right) = m*\theta-\frac{(m*\theta)^3}{3!}+\frac{(m*\theta)^5}{5!}+r*m*\theta-r*\frac{(m*\theta)^3}{3!}+r*\frac{(m*\theta)^5}{5!}+r^2*m*\theta-r^2*\frac{(m*\theta)^3}{3!}+r^2*\frac{(m*\theta)^5}{5!}+r^3*m*\theta-r^3*\frac{(m*\theta)^3}{3!}+r^3*\frac{(m*\theta)^5}{5!}+r^4*m*\theta-r^4*\frac{(m*\theta)^3}{3!}+r^4*\frac{(m*\theta)^5}{5!}+r^5*m*\theta-r^5*\frac{(m*\theta)^3}{3!}+r^5*\frac{(m*\theta)^5}{5!}$$

It can be taken into account the un-symmetric terms (odd functions) because the un-symmetric isotropic cam and ignore the symmetric terms (even functions) to obtain:

PDF created with pdfFactory Pro trial version www.pdffactory.com

$$(r^m * \sin(m*\theta)) = (r*m*\theta - \frac{(r*m*\theta)^3}{3!} + \frac{(r*m*\theta)^5}{5!}) = \sin(r*m*\theta)$$

It can be taken the first mode, m = 1:

$$(r^m * \sin(m*\theta)) = \sin(r*\theta)$$

Also the same procedure for the second term:

$$(r^{m+2} * \sin(m*\theta)) = \sin(r*\theta)$$

As before:

$$(r^m * \cos(m*\theta) = (1 + r + r^2 + r^3 + r^4 + \cdots) * (1 - \frac{(m*\theta)^2}{2!} + \frac{(m*\theta)^4}{4!} - \cdots) = 1 - \frac{(m*\theta)^2}{2!} + \frac{(m*\theta)^4}{4!} + r - r*\frac{(m*\theta)^2}{2!} + r*\frac{(m*\theta)^4}{4!} + r^2 - r^2*\frac{(m*\theta)^2}{2!} + r^2*\frac{(m*\theta)^4}{4!} + r^3 - r^3*\frac{(m*\theta)^2}{2!} + r^3*\frac{(m*\theta)^4}{4!} + r^4 - r^4*\frac{(m*\theta)^2}{2!} + r^4*\frac{(m*\theta)^4}{4!}$$

As above it can be taken into account the un-symmetric terms (odd functions) because the un-symmetric isotropic cam and ignore the symmetric terms (even functions) to obtain:

$$(r^m * \cos(m*\theta) = (1 - \frac{(r*m*\theta)^2}{2!} + \frac{(r*m*\theta)^4}{4!}) = \cos(r*m*\theta)$$

It can be taken the first mode m = 1:

$$(r^m * \cos(m*\theta)) = \cos(r*\theta)$$

Also the same procedure for the second term:

$$(r^{m+2} * \cos(m*\theta)) = \cos(r*\theta)$$

The homogenous solution of eq. (7) will become:

$$w(r,\theta)_H = A*\sin(r*\theta) + B*\cos(r*\theta) \quad , [13] \qquad (8)$$

Where:

A and B are constants.

It can be derived the homogenous solution (1, 2, 3, 4) times with respect to r and θ to obtain:

$$\frac{\partial w}{\partial r} = A*\theta*\cos(r*\theta) - B*\theta*\sin(r*\theta)$$

$$\frac{\partial^2 w}{\partial r^2} = -A*\theta^2*\sin(r*\theta) - B*\theta^2*\cos(r*\theta)$$

$$\frac{\partial^3 w}{\partial r^3} = -A*\theta^3*\cos(r*\theta) + B*\theta^3*\sin(r*\theta)$$

PDF created with pdfFactory Pro trial version www.pdffactory.com

$$\frac{\partial^4 w}{\partial r^4} = A * \theta^4 * \sin(r * \theta) + B * \theta^4 * \cos(r * \theta)$$

$$\frac{\partial^4 w}{\partial r^2 \partial \theta^2} = -A * \left(-\theta^2 * r^2 * \sin(r * \theta) + 4 * \theta * r * \cos(r * \theta) + 2 * \sin(r * \theta)\right) - B * (-\theta^2 * r^2 * \cos(r * \theta) - 4 * \theta * r * \sin(r * \theta) + 2 * \cos(r * \theta))$$

$$\frac{\partial^3 w}{\partial r \partial \theta^2} = A * (-\theta * r^2 * \cos(r * \theta) - 2 * r * \sin(r * \theta)) - B * (-\theta * r^2 * \sin(r * \theta) + 2 * r * \cos(r * \theta))$$

$$\frac{\partial^2 w}{\partial \theta^2} = -A * r^2 * \sin(r * \theta) - B * r^2 * \cos(r * \theta)$$

$$\frac{\partial^4 w}{\partial \theta^4} = A * r^4 * \sin(r * \theta) + B * r^4 * \cos(r * \theta)$$

After putting the above derivatives in eq. (7) and after simplification to obtain:

$$w(r, \theta)_H = \frac{(2*\theta^3*r^2+6*r^2*\theta-\theta)}{(\theta^4*r^3+2*r^3*\theta^2+\theta^2*r-4*r+r^3)} * A * \cos(r * \theta) - \frac{(2*\theta^3*r^2+6*r^2*\theta-\theta)}{(\theta^4*r^3+2*r^3*\theta^2+\theta^2*r-4*r+r^3)} * B * \sin(r * \theta) \tag{9}$$

And the particular solution is, [13]:

$$w(r, \theta)_P = \sum_{m_1=1,3,5}^{\infty} [C * r^4 * \sin(m * \theta)] \tag{10}$$

Applying the infinite series on the particular solution as below:

$$r^4 * \sin(m * \theta) = (1 + r + r^2 + r^3 + r^4 + \cdots) * \left(m * \theta - \frac{(m*\theta)^3}{3!} + \frac{(m*\theta)^5}{5!}\right) = m * \theta - \frac{(m*\theta)^3}{3!} + \frac{(m*\theta)^5}{5!} + r * m * \theta - r * \frac{(m*\theta)^3}{3!} + r * \frac{(m*\theta)^5}{5!}$$

Ignoring the higher order terms of the above series and applying the symmetric and un-symmetric terms:

$$r^4 * \sin(m * \theta) = r * m * \theta$$

It can be taken the first mode, m = 1:

The particular solution of eq. (7) will become:

$$w(r, \theta)_P = C * r * \theta \tag{11}$$

Substituting eq. (11) into plate equation eq. (7) and finding the value of constant (C):

$$C = \frac{q*r^3}{\theta*D}$$

$$w(r, \theta)_P = \frac{q*r^4}{D} \tag{12}$$

PDF created with pdfFactory Pro trial version www.pdffactory.com

The complementary solution of deflection is as below:

$$w(r,\theta) = w(r,\theta)_H + w(r,\theta)_P$$

$$w(r,\theta) = \frac{(2*\theta^3*r^2+6*r^2*\theta-\theta)}{(\theta^4*r^3+2*r^3*\theta^2+\theta^2*r-4*r+r^3)} * A * \cos(r*\theta) - \frac{(2*\theta^3*r^2+6*r^2*\theta-\theta)}{(\theta^4*r^3+2*r^3*\theta^2+\theta^2*r-4*r+r^3)} * B * \sin(r*\theta) + \frac{q*r^4}{D} \qquad (13)$$

Applying the boundary conditions to eq. (13), the constants (A and B) can be obtained:

At $r = r_1 = 2.5\text{ cm}, \theta = \theta_1, w(r,\theta) = 0$

At $r = r_1 = 2.5\text{ cm}, \theta = \theta_2, w(r,\theta) = 0$

Where: θ_1 and θ_2 vary along each flank and nose profile.

Then;

$$A = \frac{C_1*C_3*\sec(r_1*\theta_2)*\cos(r_1*\theta_1)*\tan(r_1*\theta_2)-C_2*C_3*\tan(r_1*\theta_2)}{C_1*C_2*(\tan(r_1*\theta_2)*\cos(r_1*\theta_1)-\sin(r_1*\theta_1))} - \frac{C_3*\sec(r_1*\theta_2)}{C_2}$$

$$B = \frac{C_1*C_3*\sec(r_1*\theta_2)*\cos(r_1*\theta_1)-C_2*C_3}{C_1*C_2*(\tan(r_1*\theta_2)*\cos(r_1*\theta_1)-\sin(r_1*\theta_1))}$$

Where:

$$C_1 = \frac{2*\theta_1^3*r_1^2+6*r_1^2*\theta_1-\theta_1}{\theta_1^4*r_1^3+2*r_1^3*\theta_1^2+\theta_1^2*r_1-4*r_1+r_1^3}$$

$$C_2 = \frac{2*\theta_2^3*r_1^2+6*r_1^2*\theta_2-\theta_2}{\theta_2^4*r_1^3+2*r_1^3*\theta_2^2+\theta_2^2*r_1-4*r_1+r_1^3}$$

$$C_3 = \frac{q*r_1^4}{D}$$

$$\therefore w(r,\theta) = \frac{(2*\theta^3*r^2+6*r^2*\theta-\theta)}{(\theta^4*r^3+2*r^3*\theta^2+\theta^2*r-4*r+r^3)} * \left[\frac{C_1*C_3*\sec(r_1*\theta_2)*\cos(r_1*\theta_1)*\tan(r_1*\theta_2)-C_2*C_3*\tan(r_1*\theta_2)}{C_1*C_2*(\tan(r_1*\theta_2)*\cos(r_1*\theta_1)-\sin(r_1*\theta_1))} - \frac{C_3*\sec(r_1*\theta_2)}{C_2}\right] * \cos(r*\theta) - \frac{(2*\theta^3*r^2+6*r^2*\theta-\theta)}{(\theta^4*r^3+2*r^3*\theta^2+\theta^2*r-4*r+r^3)} * \left[\frac{C_1*C_3*\sec(r_1*\theta_2)*\cos(r_1*\theta_1)-C_2*C_3}{C_1*C_2*(\tan(r_1*\theta_2)*\cos(r_1*\theta_1)-\sin(r_1*\theta_1))}\right] * \sin(r*\theta) + \frac{q*r^4}{D}$$

….(14)

It can be assumed that the two points of contact load are as the simply-supported beam subjected to distributed load (P_o) per unit length of point loading on the projected area (a * b), then:

PDF created with pdfFactory Pro trial version www.pdffactory.com

$$q = P_o * \frac{2*\pi}{3} * \frac{L^2}{8} * \frac{1}{L_1} \qquad ....(15)$$

Where:

L: is the length of simply-supported beam.

L_1:is the difference length between two points of contact.

In this study the cam profile boundary contains from three flanks and two noses with its dimensions, [10], as illustrated in Fig. (1); but it can be applied the equation of circular plate on (flank no.2 and a part of nose no.1) and (flank no.3 and a part of nose no.2) to obtain the value of deflection. Also the deflection of (flank no.1, a part of nose no.1, and a part of nose no. 2) can be found using the superposition theorem with the cam profile points as indicated in Fig. (2) By applying the elliptic and the semi-circle plate equations as below, [13]:

The elliptic equation is:

$$w(x,y) = \frac{q*a_1^4*b_1^4}{8*D} * \frac{(\frac{x^2}{a_1^2}+\frac{y^2}{b_1^2}-1)^2}{(3*a_1^4+3*b_1^4+2*a_1^2*b_1^2)} \qquad (16)$$

Where: a_1 and $b_1$is the major and minor distance axis of ellipse.

And the semi-circle equation i:

$$w(r,\theta) = \sum_{m_1=1,3,5}^{\infty}[\frac{4*q*r^4}{\pi*m_1*(16-m_1^2)*(4-m_1^2)*D} + A_{1m_1} * r^{m_1} + A_{3m_1} * r^{m_1+2}] * \sin(m_1*\theta) \qquad (17)$$

Where:

$$A_{1m_1} = \frac{-2*q*(m_1+1)*a_2^{4-m_1}}{\pi*m_1*(16-m_1^2)*(4-m_1^2)*D}$$

$$A_{3m_1} = \frac{2*q*(m_1-1)*a_2^{2-m_1}}{\pi*m_1*(16-m_1^2)*(4-m_1^2)*D}$$

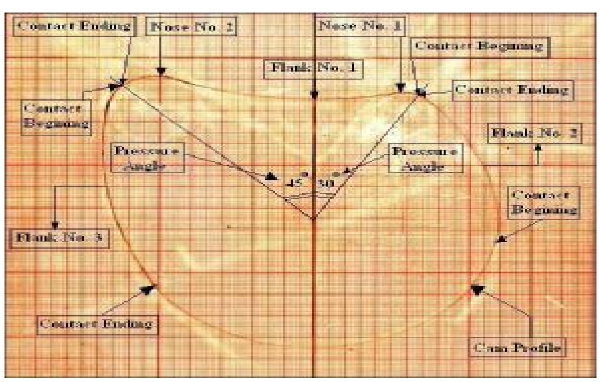

Figure (1) Cam Profile Specifications.

PDF created with pdfFactory Pro trial version www.pdffactory.com

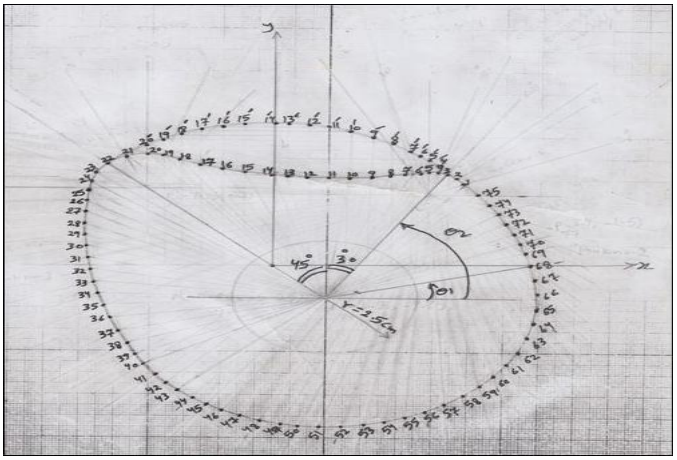

Figure (2) The Points of Cam Profile with superposition theorem.

Numerical procedure:

For comparison, a static analysis was carried out with ANSYS Program software. The linear elastic isotropic model is used to investigate the deflection on cam profile boundaries. For this problem, the (SHELL 99) element is used. This element is used for the two-dimensional modeling of shell structure and is defined by eight nodes having six degrees of freedom at each node: translations in the nodal x, y, and z directions and rotations about the nodal x, y, and z axes. The mesh generation of cam profile can be shown in Fig. (3).

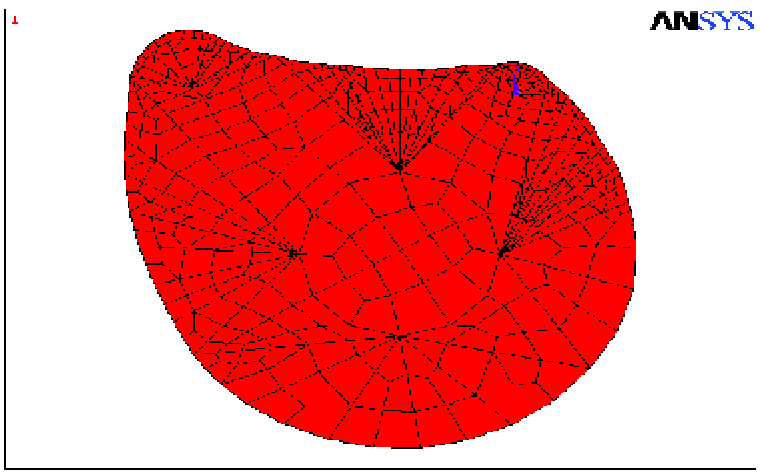

Figure (3) The mesh generation of cam un-symmetric cam profile.

PDF created with pdfFactory Pro trial version www.pdffactory.com

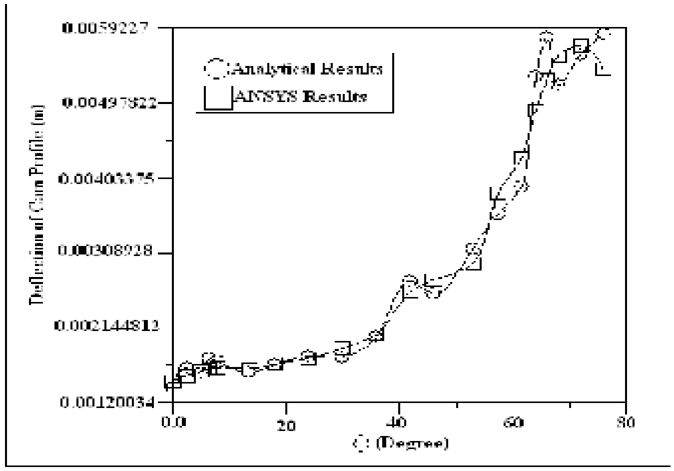

Figure (4) Deflection of cam profile against angle of contact for nose no. 1, flank no.1, and nose no. 2.

Figure (4) shows the deflection of cam profile against angle of contact for nose no. 1, flank no.1, and nose no. 2. The deflection of cam profile increases with the increasing of the angle of contact. The values of deflection of flank no. 1 vary randomly because the curve degree of flank no.1 is very high than nose no. 1 and nose no. 2.

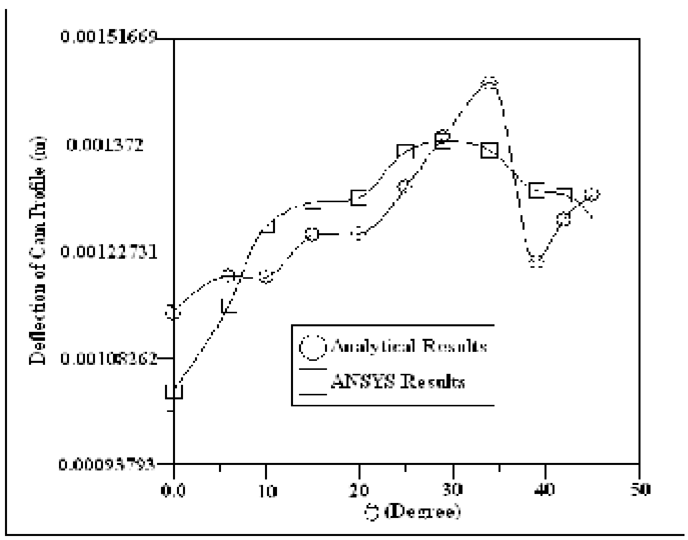

Figure (5) Deflection of cam profile against angle of contact for flank no. 2 and nose no. 1.

Figure. (5) shows the deflection of cam profile against angle of contact for flank no. 2 and nose no. 1. The deflection of cam profile vary sinosoidaly with the angle of contact for flank no. 2 and nose no. 1 because the contact loading vary sinosoidaly at cam profile boundary. The percentage error between of deflection

PDF created with pdfFactory Pro trial version www.pdffactory.com

obtainedfrom the analytical results and ANSYS results is very high than Fig. (4) because the difference in length between two points of contact (L_1) is not accurate.

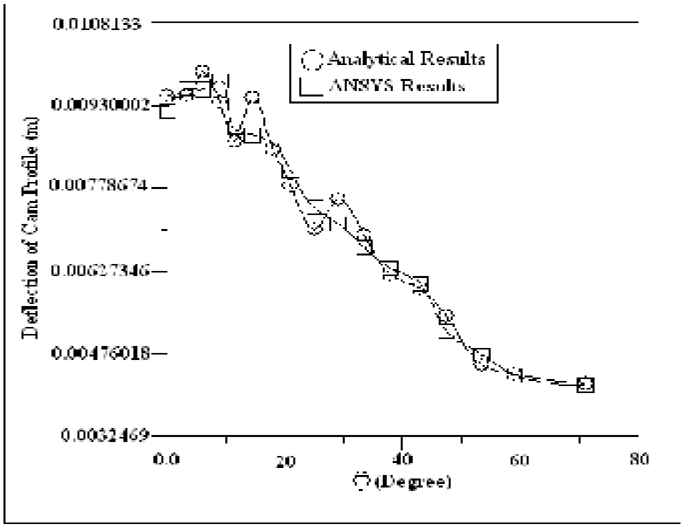

Figure (6) Deflection of cam profile against angle of contact for nose no. 2 and flank no. 3.

Fig. (6) shows the deflection of cam profile against angle of contact for nose no. 2 and flank no. 3. The values of deflection decrease with the increasing of the angle of contact because the contact loading decreases with the increasing of the angle of contact.

Table (2) The values of deflection varies with point's number of nose no. 1, flank no.1, and nose no. 2 for the un-symmetric pressure angle from the beginning and the ending points of contact.

Points Number	Analytical Results (m)	ANSYS Results (m)	Error (%)
3	0.00120034	0.0012824	6.3989 %
4	0.0014627	0.0013535	7.4656 %
5	0.0013924	0.0014197	1.9229 %
6	0.0015784	0.0014434	8.5529 %
7	0.0015447	0.0014636	5.2502 %
8	0.00140015	0.0014526	3.6107 %
9	0.00149682	0.0015132	1.0824 %
10	0.00161237	0.0015879	1.5176 %

PDF created with pdfFactory Pro trial version www.pdffactory.com

11	**0.00160498**	**0.0017259**	**7.0062 %**
12	**0.00187767**	**0.0019148**	**1.9391 %**
13	**0.002625078**	**0.0024764**	**5.6637 %**
14	**0.00245408**	**0.0026312**	**6.7315 %**
15	**0.003052388**	**0.0028545**	**6.4830 %**
16	**0.003525277**	**0.0037995**	**7.2173 %**
17	**0.003883302**	**0.0042693**	**9.0412 %**
18	**0.005356948**	**0.0049005**	**8.5206 %**
19	**0.005874945**	**0.0053147**	**9.5361 %**
20	**0.005239998**	**0.0056304**	**6.9338 %**
21	**0.005647505**	**0.0057659**	**2.0533 %**
22	**0.0059227**	**0.0054491**	**7.9963 %**

Table (2) shows the values of deflection varies with point's number of nose no. 1, flank no.1, and nose no. 2 for the un-symmetric pressure angle from the beginning and the ending points of contact. The deflection of cam boundary profile increased transiently with the increasing of point's number on cam boundary because varying the radius of curvature at these points from the point of beginning at nose no.1 to the point of ending at nose no. 2.

Table (3) The values of deflection varies with point's number of flank no. 2 and nose no. 1 of the un-symmetric pressure angle from the beginning and the ending points of contact.

Points Number	**Analytical Results (m)**	**ANSYS Results (m)**	**Error (%)**
68	**0.0010844**	**0.00093793**	**13.507 %**
69	**0.00115413**	**0.0010993**	**4.7507 %**
70	**0.00115213**	**0.0012491**	**7.7631 %**
71	**0.00123124**	**0.0012932**	**4.7912 %**
72	**0.00123323**	**0.0013015**	**5.2454 %**
73	**0.00132137**	**0.0013883**	**4.821 %**

PDF created with pdfFactory Pro trial version www.pdffactory.com

74	**0.00141482**	**0.0014082**	**0.4679 %**
75	**0.00151669**	**0.00139**	**8.353 %**
1	**0.0011806**	**0.0013155**	**10.2546 %**
2	**0.00126109**	**0.0013071**	**3.52 %**
3	**0.00130718**	**0.0012628**	**3.3951 %**

Table (3) shows the values of deflection varies with point's number of flank no. 2 and nose no. 1 of the un-symmetric pressure angle from the beginning and the ending points of contact. The deflection of cam boundary profile increased transiently with the increasing of point's numbers on cam boundary and then the deflection can be decreased because varying the radius of curvature at these points from the point of beginning at flank no. 2 to the point of ending at nose no. 1. The percentage errors is very high in some locations because the contact beginning of the un-symmetric isotropic cam.

Table (4) The values of deflection varies with point's number of nose no. 2 and flank no. 3 of the un-symmetric pressure angle from the beginning and the ending points of contact.

Points Number	**Analytical Results (m)**	**ANSYS Results (m)**	**Error (%)**
22	**0.01025422**	**0.0098552**	**3.8912 %**
23	**0.0102533**	**0.010417**	**1.5714 %**
24	**0.0108133**	**0.010394**	**3.8776 %**
25	**0.0100656**	**0.010599**	**5.0325 %**
26	**0.009128903**	**0.0094546**	**3.4448 %**
27	**0.0101918**	**0.0092871**	**8.8767 %**
28	**0.0089525**	**0.0090685**	**1.2791 %**
29	**0.00804704**	**0.0084081**	**4.2942 %**
30	**0.00701183**	**0.007521**	**6.7699 %**
31	**0.0077291**	**0.0071413**	**7.605 %**
32	**0.006876**	**0.006573**	**4.4066 %**

PDF created with pdfFactory Pro trial version www.pdffactory.com

33	**0.0059147**	**0.0060641**	**2.4636 %**
34	**0.00556022**	**0.0056907**	**2.2928 %**
35	**0.00490119**	**0.0045391**	**7.3877 %**
36	**0.00372417**	**0.0039719**	**6.237 %**
37	**0.00349276**	**0.003474**	**0.5371 %**
39	**0.00328746**	**0.0032469**	**1.2337 %**

Table (4) shows the values of deflection varies with point's number of nose no. 2 and flank no. 3 of the un-symmetric pressure angle from the beginning and the ending points of contact. The deflection of cam boundary profile decreased transiently with the increasing of point's number on cam boundary because varying the radius of curvature at these points from the point of beginning at nose no. 2 to the point of ending at flank no. 3.

CONCLUSIONS

(1) The deflection of cam profile was increased because the radius of curvature and angle of contact were increased.
(2) The contact loading is approximately constant for each nose and flank of cam profile because the radius of curvature is constant.
(3) The maximum deflection will occur at the nose no.2 having maximum pressure angle (45^o) of un-symmetric cam profile.
(4) There is no deflection on the points of duel region profile because the radius of curvature, force, and acceleration were zero.

REFERENCES

[1]Lampinen J., "Cam Shape Optimization by Genetic Algorithm ", Journal of Computer-Aided Design, No. 35, 2003, p.p. 727-737.
[2] Sanjib Acharyya, and Tarun Kanti Naskar, "Fractional Polynomial Mod Traps for Optimization of Jerk and Hertzian Contact Stress in Cam Surfaces ", Journal of Computers and Structures, No.86, 2008, p.p. 322-329.
[3] Mandal M., and Naskar T.K., " Introduction of Control Points in Splines for Synthesis of Optimized Cam Motion Program ", Journal of Mechanism and Machine Theory, No. 44, 2009, p.p. 255-271.
[4] James F. Wilson, " Impact-Induced Fatigue of Foamed Polymers ", Journal of Impact Engineering, No. 34, 2007, p.p. 1370-1381.
[5] Sateesh N., Rao C. S. P., and Janardhan Reddy T. A., " Optimization of Cam-Follower Motion Using B-Splines ", Journal of Computer Integrated Manufacturing, Vol. 22, Issue 6, June 2009, p.p. 515-523.
[6] Long-long Wu, Chun-Hsien Liu, Kuan-Lwun Shu, and Sun-Liang Chou, " Disk Cam Mechanisms with a Translating Follower having Symmetrical Double Rollers ", Journals of Mechanisms and Machine Theory, No. 44, 2009, p.p. 2085-2097.

PDF created with pdfFactory Pro trial version www.pdffactory.com

[7] Naskar T. K., and Ascharyya S., "Measuring Cam-Follower Performance ", Journal of Mechanisms and Machine Theory, No. 45, 2010, p.p. 678-691.
[8] Vu-Thinh Nguyen, and Do-Joong Kim, " Flexible Cam Profile Synthesis Method using Smoothing Spline Curves ", Journal of Mechanisms and Machine Theory, No. 42, 2007,p.p. 825-838.
[9] Jae-Gwan Kang, and Sangbo Han, "Measurement and Evaluation of Form Deviation Error of Disk Cam with an Exclusively Built Profile-Measuring Machine ", Journal of Robotics and Computers-Integrated Manufacturing, 30 March 2010, p.p. 631-701.
[10] Yu and H P Lee, "Size Optimization of Cam Mechanisms with Translating Roller Followers", Journal of Mechanical Engineering Science, Vol. 212, No. C5, 1998.
[11] Hearn E. J., "Mechanics of Materials", Book of second edition, Volume 2, 1985.
[12] Bairagi N. K., “text book of plate analysis”, 15th August, 1986.
[13] TIMOSHENKO S. and WOINOWSKY-KRIEGE S., “Theory of Plates and Shells”, McGRAW-HILL Book of second edition, 1959.

PDF created with pdfFactory Pro trial version www.pdffactory.com